Journal of Colloid and Interface Science 369 (2012) 184–192

Contents lists available at SciVerse ScienceDirect

Journal of Colloid and Interface Science

www.elsevier.com/locate/jcis

Time-resolved small angle X-ray scattering study of sol–gel precursor solutions of lead zirconate titanate and zirconia

Tomasz M. Stawski [a], Rogier Besselink [a], Sjoerd A. Veldhuis [a], Hessel L. Castricum [b], Dave H.A. Blank [a], Johan E. ten Elshof [a,*]

[a] *MESA⁺ Institute for Nanotechnology, University of Twente, P.O. Box 217, 7500 AE Enschede, The Netherlands*
[b] *Van't Hoff Institute for Molecular Sciences, University of Amsterdam, Science Park 904, 1098 XH Amsterdam, The Netherlands*

ARTICLE INFO

Article history:
Received 17 October 2011
Accepted 11 December 2011
Available online 17 December 2011

Keywords:
Lead zirconate titanate
Zirconia
PZT
Sol–gel
SAXS

ABSTRACT

The evolution of nanostructure in sol–gel derived lead zirconate titanate (PZT) and zirconia precursor sols at different hydrolysis ratios was investigated by small angle X-ray scattering (SAXS). The shape of the clusters in the zirconia sol could be described by the length-polydisperse cylindrical form factor. The zirconia-based clusters were characterized by a cross-sectional radius, r_0, of 0.28 nm and a practically monodisperse length of *ca.* 1.85 nm. These clusters were probably constructed of zirconia-related tetrameric building blocks. Similar cylindrical structural motifs were observed in PZT precursor sols with $[H_2O]/[Zr + Ti] = 9.26$ and 27.6, but the polydispersity in length was much higher. Clear scattering contributions from Ti and Pb centers were not detected, which was interpreted in terms of a homogeneous distribution of unbound lead ions in solution and the relatively low scattering intensity from any Ti-based clusters or oligomers that may have been present in the sols.

1. Introduction

Lead zirconate titanate ($PbZr_{1-x}Ti_xO_3$; PZT) is a technologically important ceramic material mainly due to its large remnant polarization, low coercive field, and high piezoelectric coefficients. It is applicable in a wide range of applications, many of which are based on the use of PZT thin films. Therefore, various thin film fabrication methods have been extensively studied [1–4]. Most common are metal–organic chemical vapor deposition (MOCVD) [5,6], sputtering [7,8], and pulsed laser deposition for the deposition of thin films of PZT [9,10]. On the other hand, chemical solution deposition techniques (CSD) [11], including the sol–gel routes [12,13], and metal–organic deposition (MOD) [14,15] have been successfully employed to fabricate PZT thin films. The sol–gel technique has attracted considerable attention because of its simplicity, low cost, good compositional control, and its potential for large area film fabrication [16].

The properties of sols are controlled by the nature of metal-carrying reagent, solvent, reagent concentration, water concentration, method of water addition, catalyst, solution preparation/reaction conditions, and other factors [11,12]. Typically, PZT sol–gel solutions consist of Ti(IV) and Zr(IV) alkoxides and either Pb(II) or Pb(IV) carboxylate precursors, solvents, water, and a catalyst. Acetic acid acts as a key chelating agent, affecting the reactivity and promoting esterification reactions that result in many alkyl acetate esters as byproducts. Metal oxoacetates and/or metal alkoxy acetates are formed due to (partial) exchange of alkoxy ligands by acetate [17]. Most metal alkoxides or metal carboxylates and oxocarboxylates can form oligomeric structures in appropriate solvents. Well-known examples are $Ti_6(O^iPr)_{10}(OOCCH_3)_4O_4$, $Ti_6(O^iPr)_8(OOCCH_3)_8O_4$, and $Zr_4O(OPr)_{10}(CH_3COCH_2COCH_3)$ [11,12]. Several complexes of Pb and Ti or Zr precursors in similar solvents have also been reported [18–22]. All of these complexes formed in the absence of water, that is, without the hydrolysis step that is typical for initiating sol–gel condensation processes.

In the "classical" sol–gel process, an alcohol, for example, 2-methoxyethanol, is used as primary solvent for the dissolution and stabilization of the three elemental metal components. In the case of PZT, a combined Pb–Ti–Zr alkoxide is known to form [11,12,16,17,23–26]. Alternatively, in the chelating method, Pb(II) or Pb(IV) acetate is dissolved in acetic acid prior to mixing with alkoxides that have been modified by, for instance, 2-methoxyethanol. In this case, acetic acid is also known to chelate metal centers in alkoxides, leading to the formation of metal oxoacetates [11–13,17,23,24,27–29]. A derivative of the latter sol preparation method was utilized in the experiments described in this paper. In particular, we focused on a PZT model solution that has been used successfully to imprint PZT nanopatterns with a lateral resolution below 200 nm by soft lithography [30]. We showed elsewhere that nanocrystalline ZrO_2 domains of 2–10 nm develop in drying thin films of similar PZT model sols [31].

* Corresponding author. Fax: +31 53 489 2990.
E-mail address: j.e.tenelshof@utwente.nl (J.E. ten Elshof).

0021-9797/$ - see front matter © 2011 Elsevier Inc. All rights reserved.
doi:10.1016/j.jcis.2011.12.033

It is known that the nature of the sol has a profound effect on the microstructure, orientation, and electrical properties of the films [12,16,26]. But despite various studies involving nuclear magnetic resonance [17,27,32–34], Fourier transform infrared spectroscopy [33,34], gas chromatography–mass spectroscopy [32], photon correlation spectroscopy [27–29], and small angle X-ray scattering [27–29], relatively few details are known about the structural evolution of PZT sols, especially where it concerns the quantitative microstructural parameters of sols and their relationship to measurable chemical properties.

Pioneering SAXS studies of alkoxide-carboxylate PZT precursor sols with a Pb/Ti/Zr ratio of 100:70:30 suggest that rod-like structures constitute an important structural motif of lead zirconate titanate and lead zirconate precursor sols [27–29]. The radii of gyration were determined from fits of the experimental data to the Guinier approximation and were found to be 4–5 nm [28]. Rod lengths were calculated by fitting to a simple Guinier approximation for rod-like particles and were in the range of 6–8 nm [29]. However, the validity of this analysis depends on the absence of polydispersity in the rod lengths [28], which cannot be assumed *a priori* in such relatively complex solutions. The absence of clearly linear regions in a number of Guinier plots [28,29] suggests that the actual structure in solution may be more complicated than was initially concluded. The authors speculated on the formation of core–shell structures [29], but no features of a core–shell morphology were identified in the scattering curves.

The aim of this study was to investigate the structure of relatively similar sol–gel PZT model solutions on a nanometer-length scale in more detail. The hydrolysis step was introduced in order to initiate the structural evolution of sols. We used *in situ* small angle X-ray scattering to investigate the evolution of PZT after hydrolysis in solutions containing stoichiometric ratios of Pb, Zr, and Ti and compared the results with scattering curves from zirconia precursor sols. We used a length-polydisperse cylinder model to fit the experimental data and compared them with a Guinier approximation for rod-like particles.

2. Experimental

2.1. Synthesis of lead zirconate titanate (PZT) precursor sols

Lead(II) acetate trihydrate (99%, Sigma–Aldrich), zirconium(IV) *n*-propoxide (70% w/w in *n*-propanol, Alfa Aesar), and titanium(IV) *iso*-propoxide (99.999%, Sigma–Aldrich) were used as precursor materials. Glacial acetic acid (99.8%, Acros) and 2-methoxyethanol (>99.3%, Sigma–Aldrich) were used as solvents, stabilizers, and chelating agents. Three stock solutions were made, each with a concentration of 0.60 mol/dm^3. A Pb-acetate solution was prepared by dissolving lead(II) acetate trihydrate in acetic acid and subsequent refluxing at 105 °C for 8 h to remove all remaining water. The other two solutions were based on titanium *iso*-propoxide and zirconium *n*-propoxide, respectively, with 2-methoxyethanol as solvent. They were stirred in a glove box under nitrogen atmosphere at room temperature for 24 h and then stored at room temperature until further use. Prior to the experiments, the stock solutions were mixed in the appropriate molar ratios and stirred for 5–10 min. The Ti and Zr stock solutions were first mixed and added to the lead acetate solution. The molar ratio Pb/Zr/Ti was always kept at 100:52:48, yielding a concentration of 0.30 mol/dm^3 in the final PZT solution. Solutions of this concentration were used in all experiments. Hydrolysis was initiated by addition of water immediately after the three stock solutions had been mixed. Two hydrolysis ratios were investigated, namely $[H_2O]/[Ti + Zr] = 9.26$ and 27.6.

2.2. Synthesis of zirconia precursor sol

Zirconium(IV) *n*-propoxide (70% w/w in *n*-propanol, Alfa Aesar) was used as precursor. Glacial acetic acid (99.8%, Merck) and 2-methoxyethanol (99.3%, Sigma–Aldrich) were used as chelating agents, solvents, and stabilizers. Zirconium(IV) *n*-propoxide was dissolved in 2-methoxyethanol and stirred in a glove box under nitrogen atmosphere, yielding a 1.00 mol/dm^3 stock solution. Then, the zirconium(IV) *n*-propoxide stock solution was mixed with acetic acid, yielding a 0.67 mol/dm^3 solution. Finally, the solution was hydrolyzed at $[H_2O]/[Zr] = 5$.

2.3. Time-resolved small angle X-ray scattering of PZT and zirconia sols

SAXS experiments were performed on the Dutch–Belgian beamline (DUBBLE) BM-26B of the ESRF in Grenoble, France [35]. The beam was focused at the corner of a 2D gas-filled multiwire detector in order to maximize the range of accessible q values (scattering vector values). The beam energy was 16 keV ($\lambda = 0.0776$ nm). The samples were placed at a distance of 1.5 m from the detector, and the intensity was measured in the range $0.13 < q < 8.42$ nm^{-1}. The raw data were corrected for the pixel-dependent detector sensitivity and integrated for channels with the same q values. To investigate *in situ* the evolution of PZT and zirconia precursor sols at elevated temperatures, SAXS data were collected on sols in lithium borate beryllium oxide glass sealed capillaries (Ø = 1.0 mm, glass no. 14, Hilgenberg, Malsfeld, Germany) that were mounted into a thermostat (Linkam), which was operated at 60 °C. Measurements were taken with 2–5 min intervals for time periods of typically 1 h.

3. Analysis of SAXS data

In SAXS experiments, the elastic scattering of X-rays by a sample that has local fluctuations in its electronic density is recorded at very small angles. Structural information about entities with dimensions <50 nm such as colloids and powders can be derived from the used angular range [36–39]. In a typical SAXS experiment, the scattering intensity $I(q)$ is plotted versus the scattering vector q (nm^{-1}), which is related to the scattering angle 2θ and the wavelength λ (nm) of the incident beam via

$$q = 4\pi/\lambda \sin\theta \tag{1}$$

In general, the scattering amplitude A in a given direction from an object of electron density $\rho(\boldsymbol{r})$ is expressed by Eq. (2) [36,38]:

$$A(\boldsymbol{q}) = \int \rho(\boldsymbol{r}) e^{-i\boldsymbol{q}\boldsymbol{r}} d\boldsymbol{r} \tag{2}$$

Hence, the scattered intensity in the direction defined by a scattering vector is $I(\boldsymbol{q}) = AA^*$, where A^* is the complex conjugate of A.

3.1. Guinier approximation for rod-like particles

In the case of rod-like particles of length L and cross-sectional radius r_0, where $L \gg r_0$, the scattering amplitude $A(\boldsymbol{q})$ can be split into length-related and cross-section-related components [38]. The scattering curve $I(q)$ of a rod-like object is given by Eqs. (3) and (4), where the cross-sectional radius of gyration R_C is related to r_0 via $r_0 = 2^{1/2}R_C$.

$$I(q) = I(0) \cdot L \cdot \frac{\pi}{q} \cdot I_C(q) \tag{3}$$

$$I_C(q) \propto \exp\left(\frac{-q^2R_C^2}{2}\right) \tag{4}$$

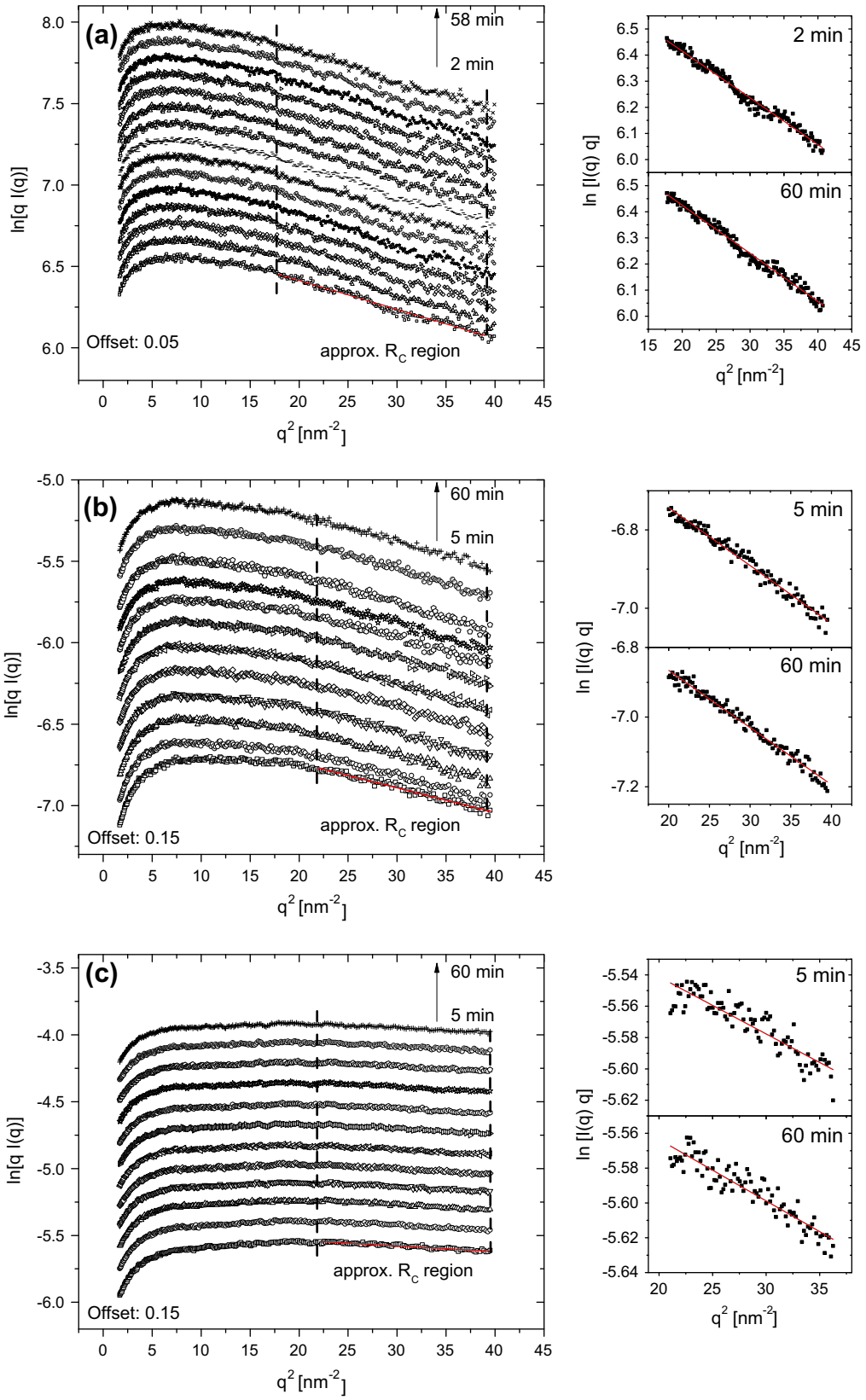

Fig. 1. ln $I(q)q$ vs. q^2 plots and exemplary linear plots from which cross-section radius of gyration, R_c, was calculated for: (a) zirconia precursor sol of initial concentration of 0.67 mol/dm^3 and hydrolyzed with $[H_2O]/[Zr] = 5$; (b) PZT precursor sol of initial concentration of 0.30 mol/dm^3 and hydrolyzed with $[H_2O]/[Ti + Zr] = 9.26$; (c) PZT precursor sol of initial concentration of 0.30 mol/dm^3 and hydrolyzed with $[H_2O]/[Ti + Zr] = 27.6$.

Eq. (4) is valid when $2\pi/L < q < 1/R_C$. The scattering intensity at zero angle is given by $I(0) = N(\Delta\rho)^2V^2$, where V is the scattering volume of a particle, N is the number density of particles, and $\Delta\rho$ is the difference between the electron density of the scattering particle and

its surrounding matrix. Eq. (4) is independent of the actual shape of the cross-section in the applicable q range, provided that the particle sizes and shapes are sufficiently monodisperse. Thus, if a given system is composed of rod-like particles of relatively monodisperse cross-sectional dimension, the plot ln $I(q)q$ vs. q^2 should show a straight line. Eq. (4) is known as the Guinier approximation for rod-like particles [36,38].

3.2. Form factor of length-polydisperse cylinders

Eqs. (3) and (4) are approximations of more rigorous expressions. For rod-like particles of length L and circular cross-section radius r_0, the cylinder form factor Eq. (5) can be used [40,41].

$$P_{cyl}(q,r_0,L)=\int_0^{\pi/2}\left[\frac{2J_1(qr_0\sin\alpha)}{qr_0\sin\alpha}\right]^2\left[\frac{\sin\left(\frac{1}{2}qL\cos\alpha\right)}{\frac{1}{2}qL\cos\alpha}\right]^2\sin\alpha d\alpha, \quad (5)$$

where $J_1(x)$ is the first order Bessel function and α is the angle between the long axis of the cylinder and the primary beam. In most systems, the polydispersity must also be taken into account. In the case of polydisperse cylinders of z-average form factor $P_z(q,r_0,L)$, the volume distribution $w(L)$ is included as in Eq. (6) [42–45]:

$$P_z(q,r_0,L)=\frac{\int_0^\infty L\cdot w(L)\cdot P_{cyl}(q,r_0,L)dL}{\int_0^\infty L\cdot w(L)dL}\Rightarrow$$
$$I(q)=I(0)\cdot P_z(q,r_0,L)$$

Due to its convenient parameterization, the Zimm–Schulz–Flory distribution Eq. (7) is used in the present work. This distribution has often been employed to analyze scattering data from ladder-like or worm-like polymers [43–45].

$$w(L)=\frac{L^z}{\Gamma(z+1)}\left(\frac{z+1}{L_w}\right)^{z+1}\exp\left(-\frac{z+1}{L_w}\cdot L\right) \quad (7)$$

Here, L_w is the weight-averaged length of the cylinders, L_n is the number-averaged length, and $z^{-1}=L_w/L_n-1$. The z-averaged length-polydisperse cylinder form factor as defined by Eqs. (5) and (6) can be partially solved analytically with respect to dL when it is combined with the Zimm–Schulz–Flory distribution, $w(L)$, of Eq. (7). The relevant equations are derived in the Supporting Information file.

The ln $I(q)q$ vs. q^2 plots were made based on Eqs. (3) and (4) to evaluate the shape of the particles and to determine values for R_C from appropriate linear regression fits. Then, based on these representations, the more advanced polydisperse cylinder models were employed. Eqs. (5)–(7) were used to fit all experimental data using the well-known Levenberg–Marquardt algorithm [46,47]. Sets of parameters $I(0)$, r_0, L_w, and z were calculated for all individual scattering curves, providing more detailed information about the dimensions and polydispersity of the particles.

4. Results and discussion

4.1. Time-resolved SAXS experiments

Fig. 1A shows plots of ln $I(q)q$ as a function of q^2 of the zirconia precursor sol. Fig. 1B and C shows similar data of PZT precursor sols with hydrolysis ratios $[H_2O]/[Ti+Zr]=9.26$ and 27.6, respectively. The insets on the right-hand side of Fig. 1A–C show linear fits to the first and last scattering curve from each series in the range $20<q^2<40$, where Eq. (4) is valid.

The linear ranges in this Guinier representation for rod-like particles ln $I(q)$ q versus q^2 in Fig. 1 indicate that all three sols consisted of anisotropic, elongated scatterers and that the scatterers in all three sols had identical cross-sectional dimensions. The cross-sectional radius of gyration R_C was calculated using Eq. (4).

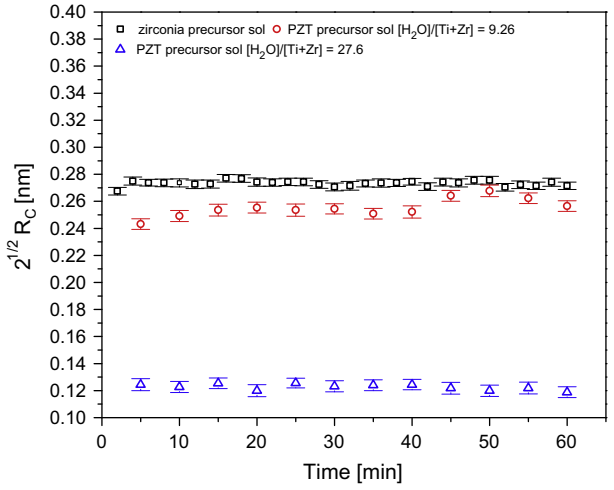

Fig. 2. Evolution of R_c as a function of time for zirconia precursor sol of initial concentration of 0.67 mol/dm^3 and hydrolyzed with $[H_2O]/[Zr]=5$; PZT precursor sol of initial concentration of 0.30 mol/dm^3 and hydrolyzed with $[H_2O]/[Ti+Zr]=9.26$; PZT precursor sol of initial concentration of 0.30 mol/dm^3 and hydrolyzed with $[H_2O]/[Ti+Zr]=27.6$. The parameter values were derived from data presented in Fig. 1.

Under the assumption that the scatterers have a circular cross-section, the factor $2^{1/2}R_C$ is plotted as a function of time in Fig. 2.

The scattering particles in the zirconia precursor sol had a constant value of $2^{1/2}R_C$ of *ca.* 0.27 nm throughout the experiment. The PZT precursor sol with $[H_2O]/[Ti+Zr]=9.26$ had a similar value of 0.24–0.27 nm, and the PZT sol with $[H_2O]/[Ti+Zr]=27.6$ had a lower value of ~0.13 nm for $2^{1/2}R_C$. The similar values and trends in R_C for the zirconia sol and the PZT precursor sol with $[H_2O]/[Ti+Zr]=9.26$ may indicate that these two sols contain very similar species in terms of dimensions and shape. Differences between the respective values are discussed below. The smaller values of R_C of the PZT sol with $[H_2O]/[Ti+Zr]=27.6$ suggest that another kind of species was formed in the precursor solution at higher hydrolysis ratio.

A more detailed analysis was carried out by fitting the experimental data with a length-polydisperse cylinder model using Eqs. (5)–(7). Different form factors were attempted in the fitting routines, such as cylinders with elliptical cross-section, elongated ellipsoids, and core–shell variations of these form factors. These analyses confirm that a cylinder form factor described the investigated structures best. The data sets of all three sols are shown on the left side in Fig. 3. Experimental data of two selected scattering curves and their best fits are presented on the right-hand side in Fig. 3.

For each scattering curve, a set of four fit parameters was determined, namely r_0 (radius of cylinder), L_w (mass-averaged cylinder length), z (a measure of the polydispersity in the length of a set of cylinders), and $I(0)$, the scattering intensity in the limit toward zero scattering angle. It is noted that all scattering curves were fitted independently from each other.

Figs. 4–6 show fitted values of r_0, L_w, and z, respectively. The latter two parameters are directly related to the polydispersity index (*PDI*), defined here as $PDI=L_w/L_n=z^{-1}+1$. The inset in Fig. 7 shows the evolution of $I(0)$ as a function of time of the same sols. Due to the fact that all three samples were measured in capillaries with slightly varying dimensions, and the SAXS patterns of the PZT and zirconia sols were measured using different calibrations of the experimental setup, the intensity is shown in arbitrary units. The values of $I(0)$ can therefore only be compared within a single measurement series, and only trends can be interpreted. However, since $I(0)=NV^2(\Delta\rho)^2$ and $V\sim r_0^2L_w$, the mass-averaged product of

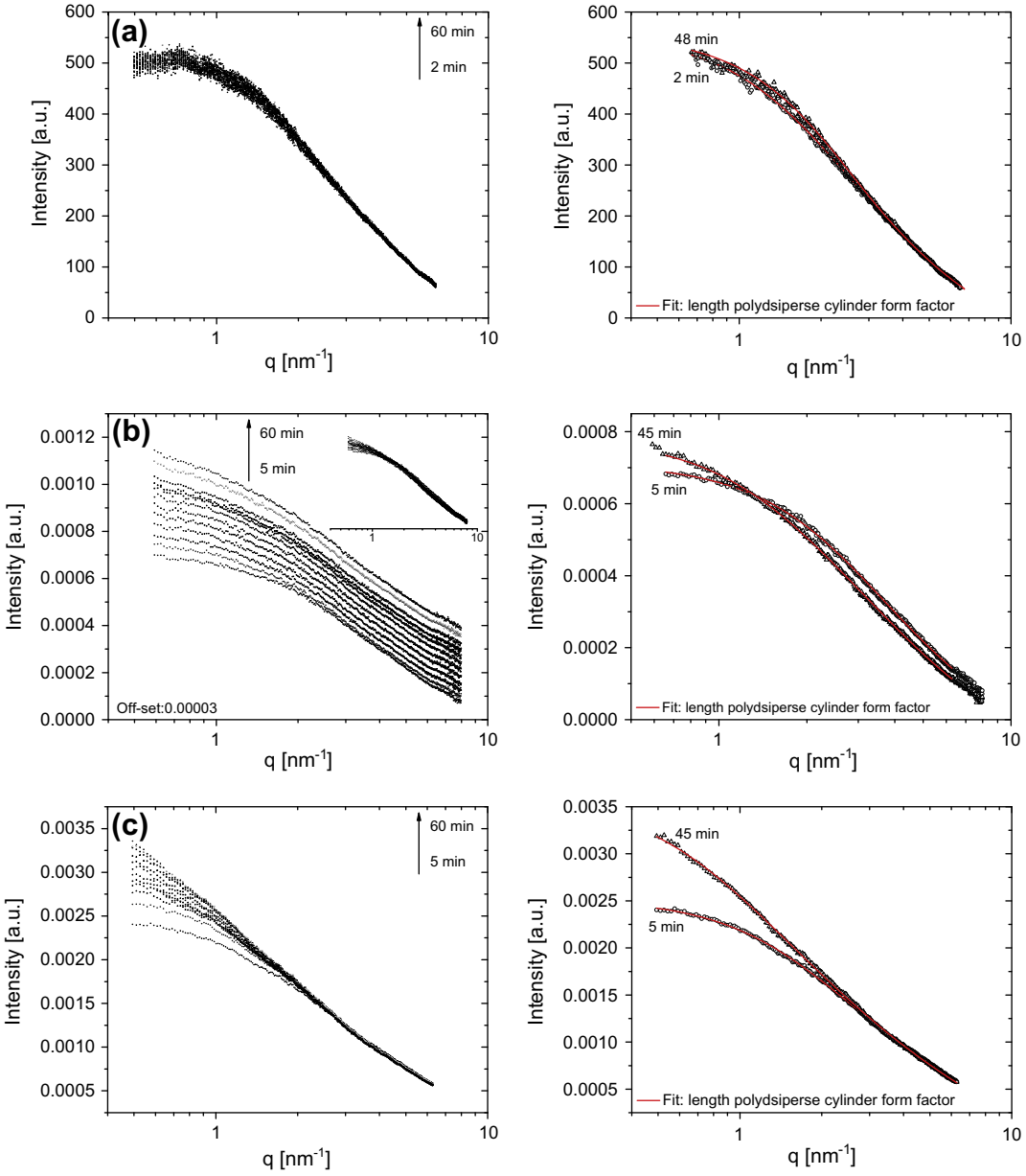

Fig. 3. Time-resolved *in situ* SAXS data of the investigated exemplary fits with the model from Eqs. (5)–(7); (a) zirconia precursor sol of initial concentration of 0.67 mol/dm^3 and hydrolyzed with [H_2O]/[Zr] = 5; (b) PZT precursor sol of initial concentration of 0.30 mol/dm^3 and hydrolyzed with [H_2O]/[Ti + Zr] = 9.26; (c) PZT precursor sol of initial concentration of 0.30 mol/dm^3 and hydrolyzed with [H_2O]/[Ti + Zr] = 27.6.

particle number density and squared electron density difference $\langle N(\Delta\rho)^2\rangle_w$ can be expressed as

$$\langle(\Delta\rho)^2 N\rangle_w = \langle I(0)V^{-2}\rangle_w \sim \langle I(0)L_w^{-2}r_0^{-4}\rangle_w \quad (8)$$

The graph in Fig. 7 presents the factor $\langle I(0)L_w^{-2}r_0^{-4}\rangle$ of all three sols as a function of time. Since it contains only N and $\Delta\rho$ as variables, $\langle I(0)L_w^{-2}r_0^{-4}\rangle$ is a measure of the number density of particles when $\Delta\rho$ can be assumed to remain constant.

4.2. Interpretation of experimental data

The SAXS patterns of the zirconia sols shared some typical characteristics with the patterns of the PZT precursor sols at $q > 2$ nm^{-1}, where part of $I(q)$ scaled with q^{-1}. We may therefore assume that the zirconium alkoxide and PZT sols also share similar structural species.

In general, no directly detectable contributions from Pb or Ti were present in the PZT SAXS patterns. The absence of a Pb signature is indicative of the very limited reactivity of lead ions under these conditions. Pb^{2+} ions are very soluble at low pH and do not condense or precipitate easily from solution until the pH increases considerably. Homogeneously dissolved Pb^{2+} ions in solution are not detectable by SAXS.

The scattering power of Ti is comparatively smaller than that of Zr due to its smaller electron density. Contributions from Ti-rich scatters might therefore be shielded by the stronger signals arising from Zr-rich scatterers. While the formation of mixed Zr/Ti alkoxoacetate structures has been reported [48], it is known that pure Ti alkoxides in an excess of acetic acid form oligomeric compounds with stoichiometry $TiO(CH_3COO)_2$ [49]. Such oligomers

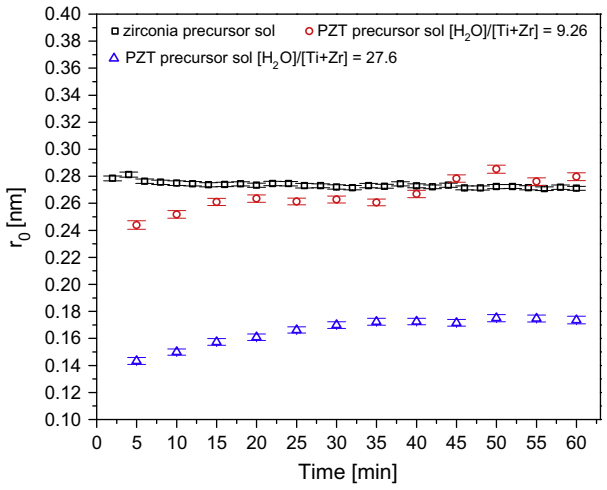

Fig. 4. Evolution of r_0 as a function of time for zirconia precursor sol of initial concentration of 0.67 mol/dm^3 and hydrolyzed with [H_2O]/[Zr] = 5; PZT precursor sol of initial concentration of 0.30 mol/dm^3 and hydrolyzed with [H_2O]/[Ti + Zr] = 9.26; PZT precursor sol of initial concentration of 0.30 mol/dm^3 and hydrolyzed with [H_2O]/[Ti + Zr] = 27.6. The parameter values were derived from the model based on Eqs. (5)–(7).

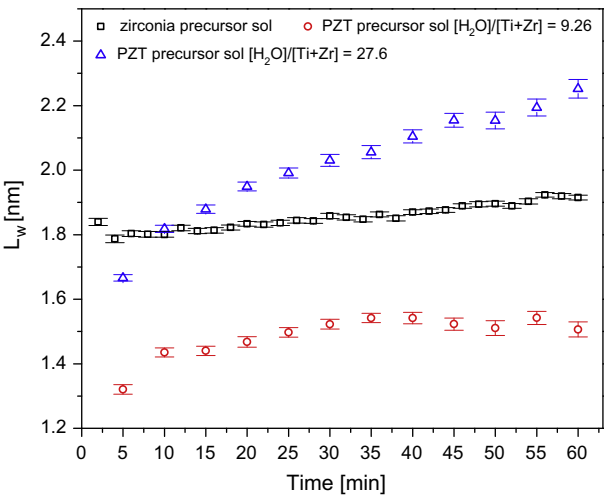

Fig. 5. Evolution of L_w as a function of time for zirconia precursor sol of initial concentration of 0.67 mol/dm^3 and hydrolyzed with [H_2O]/[Zr] = 5; PZT precursor sol of initial concentration of 0.30 mol/dm^3 and hydrolyzed with [H_2O]/[Ti + Zr] = 9.26; PZT precursor sol of initial concentration of 0.30 mol/dm^3 and hydrolyzed with [H_2O]/[Ti + Zr] = 27.6. The parameter values were derived from the model based on Eqs. (5)–(7).

would yield SAXS patterns with characteristics of fractal-like agglomerate morphologies, constructed from spherical primary scatterers [50–52]. Such patterns are quite distinct from the patterns observed in the present study.

Several small zirconium complexes have been reported. Jutson et al. conjectured from SAXS experiments the cylindrical shape of ziconia clusters and the constancy of their radius [53]. Toth et al. investigated the properties of hydrous zirconium(IV) tetramers [54]. They observed discrete $[Zr_4(OH)_8(H_2O)_{16}]^{8+}$ units derived from $Zr(NO_3)_4$ at high pH. Zirconia tetramers as building blocks of oligomeric structures were already proposed several decades earlier by Clearfield [55–57]. The authors reported an R_g of 0.46 nm and suggested that these structures have a cylindrical shape as found by SAXS. However, the accuracy of the experimental data was limited compared to today's standards. Another SAXS study on a system of zirconyl chloride revealed the coexistence of tetrameric $[Zr_4(OH)_8(H_2O)_{16}Cl_6]^{2+}$ and octameric $Zr_8(OH)_{20}(H_2O)_{24}Cl_{12}$ species at a given pH-dependent equilibrium [58], with radii of gyration of 0.37 and 0.50 nm, respectively. Growth and aggregation of zirconium hydrous polymers were extensively studied under various experimental conditions with SAXS by Singhal et al. [59] and Riello et al. [60]. Both groups found that cylinder-shaped particles of constant cross-sectional radius formed in early stages of sol development. An analogous polydisperse cylinder model was used to analyze data [60], yielding comparable results as we obtained here. The measured radius of the cylinder cross-section equaled 0.46 nm.

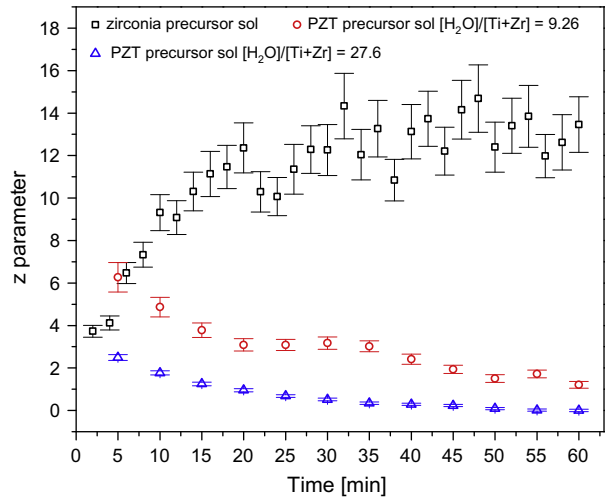

Fig. 6. Evolution of z parameter as a function of time for zirconia precursor sol of initial concentration of 0.67 mol/dm^3 and hydrolyzed with [H_2O]/[Zr] = 5; PZT precursor sol of initial concentration of 0.30 mol/dm^3 and hydrolyzed with [H_2O]/[Ti + Zr] = 9.26; PZT precursor sol of initial concentration of 0.30 mol/dm^3 and hydrolyzed with [H_2O]/[Ti + Zr] = 27.6. The parameter values were derived from the model based on Eqs. (5)–(7).

The structure of a hydroxylated zirconium tetramer was also determined by crystallographic methods and modeled by Carr–Parinello Molecular Dynamics [54,55,61]. The average Zr–Zr distance in a tetramer is equal to *ca.* 0.38 nm. It is the distance between the apexes of a square. Finally, in a SAXS study of hydrolyzed zirconium acetate xerogels, it was proposed that the primary units were cylindrical, containing either three or four cyclic tetramer units in a single plane, stacked on top of each other in the direction perpendicular to the plane [62]. Such structural motifs may be stacked into several layers forming larger cylindrical objects. Thus, our choice of length-polydispersed cylindrical form factor Eq. (5) seems to be reasonable, as this geometrical shape is a recurring structural feature of zirconia-based structures at several length scales as outlined above. If we assume that (1) a tetrameric unit constitutes a primary building block and (2) larger structures are composed of stacked tetramers, then a cylinder with a tetramer inscribed in its base would have a radius of *ca.* 0.27 nm ($r_0 = 2^{1/2}\cdot 0.38/2$ nm, see Fig. 8A), which is in close agreement with the values of $2^{1/2}R_C$ in Fig. 1A, and the r_0 parameters of the investigated zirconia sols in Fig. 4.

Zirconium is a relatively heavy element, and therefore, the scattering contrast between the organic solvent medium and the scattering entities is large. The scattering contrast between the solvent medium and the external organic ligands coordinated to zirconium is probably negligible, as they are very similar to the solvent medium. The electron density of these ligands will therefore not contribute significantly to the scattering intensity of the complex. Thus, only the central Zr-based framework contributes to scattering contrast. This may explain why the cross-sectional radius observed by us is lower than in studies where zirconia chloride, nitrate, and sulfate salts were synthesized [59,60].

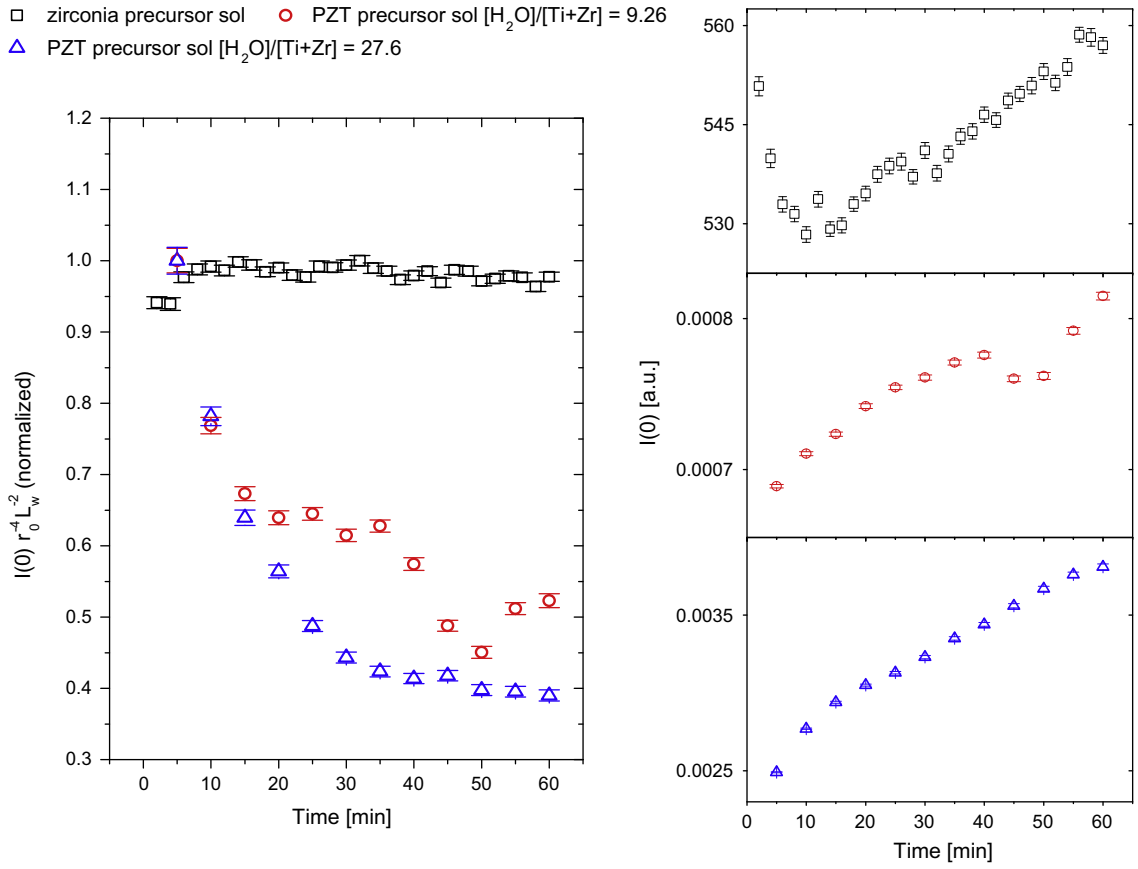

Fig. 7. Evolution of $I(0)$ divided by a mass-averaged volume of a particle as a function of time for zirconia sol, with initial concentration 0.67 mol/dm^3, [H_2O]/[Zr] = 5; PZT sol with initial concentration 0.30 mol/dm^3; [H_2O]/[Ti + Zr] = 9.26; PZT sol of initial concentration 0.30 mol/dm^3, [H_2O]/[Ti + Zr] = 27.6. The fitted parameters were derived from the model based on Eqs. (5)–(7). All values are normalized with respect to $I(0)$ at t = 5 min. Inset on the right-hand side presents $I(0)$ as a function of time for three investigated sols.

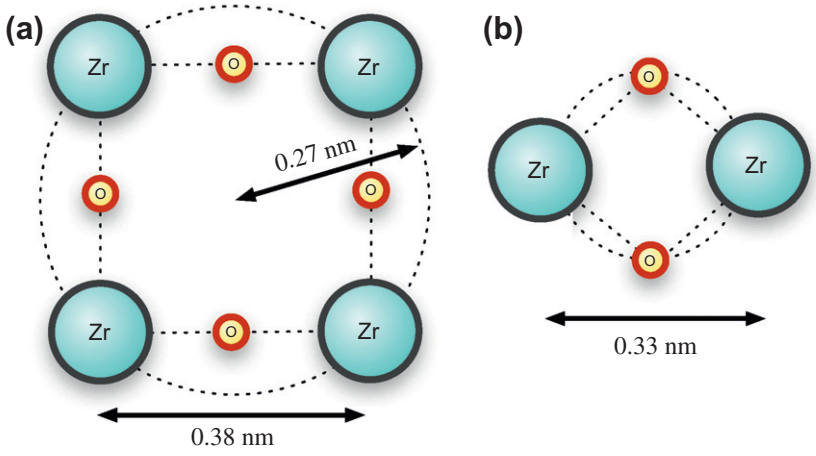

Fig. 8. Schematic representation of (a) zirconium oxo tetramer and (b) zirconium oxo dimer.

Fig. 5 shows the evolution of the mass-averaged length of cylinders in time. In the zirconia sol, L_w increased only slightly from 1.79 to 1.85 nm. Simultaneously, the z parameter increased from ~3 to a plateau at ~13 in Fig. 6. This implies that the polydispersity decreased, finally reaching PDI = 1.08. The evolution of $\langle I(0)r_0^{-4}L_w^{-2}\rangle_w$ in Fig. 7 shows that the mass-averaged product $\langle N(\Delta\rho)^2\rangle_w$ slightly increased and then reached a plateau. Since the electron density of the scattering Zr-based complexes remains virtually constant ($\Delta\rho$ is constant), the trend suggests that the number of particles N in the zirconia sol increased initially and became constant after 15 min of reaction. The high final value of z shows that polydispersity was low and indicates that only one length of cylindrical particles remained in the system by that time.

The hydrolyzed 0.3 mol/dm^3 PZT sols showed different trends. For the sol with [H_2O]/[Ti + Zr] = 9.26, the circular cross-section radii $2^{1/2}R_C$ and r_0, determined from the Guinier approximation in Fig. 2 and the cylinder model in Fig. 4, were 0.24–0.27 nm and 0.24–0.28 nm, respectively. L_w increased from 1.3 to 1.5 nm before

leveling off (Fig. 5). On the other hand, the z parameter decreased from 6.3 to 1.2, yielding $PDI = 1.83$, that is, a substantially higher polydispersity than found in the zirconia sol. The evolution of these parameters suggests that the initial structure resembled the structure of the zirconia sol. However, due to hydrolysis and the presence of Pb and Ti-containing species, not only their length but also their cross-sectional dimensions increased during growth. The normalized plot of $\langle I(0)r_0^{-4}L_w^{-2}\rangle_w$ in Fig. 7 shows a gradual decrease. Reduction of this parameter indicates reduction of the overall extent of scattering. Since its value is proportional to $N(\Delta\rho)^2$ and $\Delta\rho$ is probably constant, it follows that N probably decreased in the course of reaction, possibly due to agglomeration and growth of particles.

The PZT sol with $[H_2O]/[Ti + Zr] = 27.6$ has a smaller radius of cross-section, $2^{1/2}R_C = 0.13$ nm, as found from Eq. (4). The scattering intensity was low due to the small dimensions of the scatterers. The particle shape and an approximate value of R_C could be extracted from the experimental data, but the absolute values should be interpreted with some care. The r_0 values obtained from the length-polydisperse cylinder model are more accurate. r_0 varied from 0.145 to 0.175 nm in the first 30 min of reaction. These values are smaller than found in the zirconia and other PZT sol. This indicates that the nature of the scatterers may be different at high hydrolysis ratio, although their shape was also cylindrical. Rao et al. reported dimeric $[Zr_2(OH)_2(H_2O)_{12}]^{6+}$ and trimeric $[Zr_3(OH)_3O(H_2O)_{18}]^{7+}$ in a computational study [63]. A cylindrical structure consisting of dimers stacked in the direction perpendicular to the cyclic $Zr_2(OH)_2$ plane would have a radius $r_0 = 0.18$ nm, and stacking of dimers in their respective planes would yield a smaller r_0 (essentially a chain of Zr–O–Zr surrounded by ligands). Similar stacks of tetramers along their respective planes would yield a structure analogous to the structure of stacked zirconia dimers. However, in such a case, one would expect more a ribbon (or stiff lamella) rather than pseudo-cylinder in rotation. It is not possible to distinguish between these two situations at such small dimensions or R_C.

For the corresponding trimer-based cylinder, $r_0 = 0.20$ nm. The simulations indicated that trimetric units are less stable than dimers or tetramers. The actual Zr–Zr distance is strongly dependent on the surrounding ligands in the dimer structure, as shown by EXAFS [64]. The Zr–Zr distance in Zr(IV) *iso*-propoxide and *n*-butoxide modified with acetylacetone (acac) was 0.353 nm, independent of [Zr]/[acac] ratio. When these alkoxides were modified with acetic acid, the distances decreased to 0.335–0.339 nm at $[Zr]/[CH_3COOH] = 0.5$ [64]. These dimensions are similar to the experimental values of $r_0 = 0.145$–0.175 nm obtained in this study (Fig. 8B).

The L_w parameter ranged from 1.7 to 2.3 nm, without reaching an obvious upper limiting value. The z parameter decreased from 2.5 to 0, yielding $PDI \gg 10$, which is typical for systems with a high degree of polydispersity. Thus, a clear structural reconfiguration toward a polydisperse system of cylindrical scattering entities occurred upon hydrolysis. The plot of $\langle I(0)r_0^{-4}L_w^{-2}\rangle_w$ in Fig. 7 shows that the mass-averaged number of particles decreases. All data suggest that condensation and/or agglomeration processes take place in the solution, yielding a broad mass distribution. So while not being detectable directly, the presence of Ti and Pb affects the growth of the Zr-based phase, as reflected in the decrease of $\langle I(0)r_0^{-4}L_w^{-2}\rangle_w$ and the decrease of z in both PZT sols.

In a previous study on the microstructure of as-dried PZT precursor thin films, we found that the films contained nanocrystalline Zr-rich spherical domains of 2–10 nm diameter embedded in an amorphous matrix of Zr, Ti, and Pb [31]. Electron energy loss spectroscopy (EELS) showed that these nanocrystals contained no or a very low concentration of Ti. Probably, the cylindrical Zr-based structures that were observed in the present study are the starting nuclei for these zirconia domains. The dimensions of the scattering entities that we extracted from our data in the present study, that is, $2^{1/2}R_C < 0.5$ nm and $L_w < .5$ nm for all samples, suggest that substantial agglomeration of Zr-rich entities takes place during or after the stage in which the sol is dried as a thin film. This implies that the Zr-rich domains in as-dried films were formed in a process that was relatively isolated from the condensation of the amorphous solid phase that contained Pb, Ti, and Zr.

5. Conclusions

Cylinder-shaped particles constitute one of the primary building blocks of zirconia and lead zirconate titanate precursor sols. SAXS curves from these systems were modeled with a length-polydispersed cylinder form factor. In the zirconia sol, the particles had a radius of *ca.* 0.27 nm and a length L_w of *ca.* 1.8 nm. Such a structure can be explained in terms of a stack of cyclic zirconia tetramers. Similar structural motifs were also present in the PZT sols with $[H_2O]/[Ti + Zr] = 9.3$–27.6. These sols contained anisotropic particles with L_w values of 1.4–2.3 nm and $2^{1/2}R_c < 0.3$ nm. The number of particles in the PZT sols decreased in the course of time, while the zirconia sol seemed to converge to a stable and monodisperse state after some time. This suggests that condensation and/or agglomeration processes take place in the PZT solutions, yielding broad mass distributions of cylindrical particles based on zirconia-related structures. No direct evidence for the presence of Pb- and/or Ti-related structures was found in the investigated PZT sols.

Acknowledgments

This work was financially supported by the Netherlands Technology Foundation STW. We thank the Netherlands Organization for Scientific Research (NWO) for providing us with beam time at the ESRF DUBBLE beam line. Dr. Wim Bras and Dr. Giuseppe Portale and other beam line staff of DUBBLE are thanked for their competent support.

Appendix A. Supplementary material

Supplementary data associated with this article can be found, in the online version, at doi:10.1016/j.jcis.2011.12.033.

References

[1] J.F. Scott, C.A. Paz De Araujo, Science 246 (1989) 1400.
[2] J.F. Scott, Science 315 (2007) 954.
[3] P. Muralt, J. Micromech. Microeng. 10 (2000) 136.
[4] M. Kondo, K. Sato, M. Ishii, N. Wakiya, K. Shinozaki, K. Kurihara, Jpn. J. Appl. Phys. 45 (2006) 7516.
[5] H.R. Kim, S. Jeong, C.B. Jeon, O.S. Kwon, C.S. Hwang, J. Mater. Res. 16 (2001) 3583.
[6] Y. Otani, S. Okamura, T. Shiosaki, J. Electroceram. 13 (2004) 15.
[7] Y.C. Lin, H.A. Chuang, J.H. Shen, Vacuum 83 (2009) 921.
[8] R. Bouregba, G. Poullain, B. Vilquin, H. Murray, Mater. Res. Bull. 35 (2000) 1381.
[9] T.J. Zhu, L. Lu, M.O. Lai, Appl. Phys. A 81 (2005) 701.
[10] M. Dekkers, M.D. Nguyen, R. Steenwelle, P.M. te Riele, D.H.A. Blank, G. Rijnders, Appl. Phys. Lett. 95 (2009) 0129021.
[11] R.W. Schwartz, Chem. Mater. 9 (1997) 2325.
[12] R.W. Schwartz, T.J. Boyle, S.J. Lockwood, M.B. Sinclair, D. Dimos, C. Buchheit, Integr. Ferroelectrics 7 (1995) 259.
[13] G. Yi, M. Sayer, Ceram. Bull. 70 (1991) 1173.
[14] M. Klee, R. Eusemann, R. Waser, W. Brand, H. van Hal, J. Appl. Phys. 72 (1992) 1566.
[15] T. Cui, D. Markus, S. Zurn, D.L. Polla, Microsyst. Technol. 10 (2004) 137.
[16] R.W. Schwartz, J.A. Voigt, B.A. Tuttle, D.A. Payne, T.L. Reichert, R.S. DaSalla, J. Mater. Res. 12 (1997) 444.
[17] R.A. Assink, R.W. Schwartz, Chem. Mater. 5 (1993) 511.
[18] H.K. Chae, D.A. Payne, Z. Xu, L. Ma, Chem. Mater. 6 (1994) 875.
[19] A. Brethon, L.G. Hubert-Pfalzgraf, J. Sol–Gel Sci. Technol. 39 (2006) 159.
[20] A. Brethon, L.G. Hubert-Pfalzgraf, J.C. Daran, Dalton Trans. (2006) 250.
[21] L.G. Hubert-Pfalzgraf, S. Daniele, R. Papiernik, M.C. Massiani, B. Septe, J. Vaissermann, J.-C. Daran, J. Mater. Chem. 7 (1997) 753.

[22] S. Daniele, R. Papiernik, L.G. Hubert-Pflazgraf, S. Jagner, M. Hikansson, Inorg. Chem. 34 (1995) 628.
[23] R.W. Schwartz, T.S. Schneller, R. Waser, C.R. Chim. 7 (2004) 433.
[24] R.W. Schwartz, M. Narayanan, in: D.B. Mitzi (Ed.), Solution Processing of Inorganic Materials, John Wiley & Sons, Inc., New Jersey, 2009, p. 33.
[25] B. Malic, M. Kosec, I. Arcon, A. Kodre, J. Eur. Ceram. Soc. 25 (2005) 2241.
[26] T. Schneller, R. Waser, J. Sol–Gel Sci. Technol. 42 (2007) 337.
[27] Q. Zhang, Z. Huang, M.E. Vickers, R.W. Whatmore, J. Eur. Ceram. Soc. 19 (1999) 1417.
[28] Q. Zhang, M.E. Vickers, A. Patel, R.W. Whatmore, J. Sol–Gel Sci. Technol. 11 (1998) 141.
[29] Q. Zhang, R.W. Whatmore, M.E. Vickers, J. Sol–Gel Sci. Technol. 15 (1999) 13.
[30] S.U. Khan, O.F. Göbel, D.H.A. Blank, J.E. ten Elshof, ACS Appl. Mater. Interfaces 1 (2009) 2250.
[31] T.M. Stawski, S.A. Veldhuis, H.L. Castricum, E.G. Keim, G. Eeckhaut, W. Bras, D.H.A. Blank, J.E. ten Elshof, Langmuir 27 (2011) 11081.
[32] M. Zhang, I.M.M. Salvado, P.M. Vilarinho, A.J.D. Silvestre, A.M.S. Silva, J. Am. Ceram. Soc. 90 (2007) 358.
[33] R. Caruso, O. de Sanctis, A. Frattini, C.S.R. Gil, Surface Coat. Technol. 122 (1999) 44.
[34] T.J. Boyle, D. Dimos, R.W. Schwartz, T.M. Alam, M.B. Sinclair, C.D.J. Buchheit, J. Mater. Res. 12 (1997) 1022.
[35] W. Bras, I.P. Dolbnya, D. Detollenaere, R. van Tol, M. Malfois, G.N. Greaves, A.J. Ryan, E. Heeley, J. Appl. Crystallogr. 36 (2003) 791.
[36] A. Guinier, G. Fournet, Small Angle Scattering of X-rays, John Wiley & Sons Inc., New York, 1955.
[37] O. Kratky, in: O. Glatter, O. Kratky (Eds.), Small Angle X-ray Scattering, Academic Press, London, 1982, p. 3.
[38] G. Porod, in: O. Glatter, O. Kratky (Eds.), Small Angle X-ray Scattering, Academic Press, London, 1982, p. 17.
[39] A.F. Craievich, Mater. Res. 5 (2002) 1.
[40] G. Fournet, Bull. Soc. Fr. Minéral. Crist. 74 (1951) 39.
[41] J.S. Pedersen, Adv. Colloid Interface Sci. 70 (1997) 171.
[42] D.I. Svergun, P.V. Konarev, V.V. Volkov, M.H.J. Koch, W.F.C. Sager, J. Smeets, E.M. Blokhuis, J. Chem. Phys. 113 (2000) 1651.
[43] D. Pötschke, P. Hickl, M. Ballauff, P.-O. Åstrand, J.S. Pedersen, Macromol. Theory Simul. 9 (2000) 345.
[44] P. Hickl, M. Ballauff, U. Scherf, K. Müllen, P. Lindner, Macromolecules 30 (1997) 273.
[45] T. Sauer, G. Wegner, Macromolecules 24 (1991) 2240.
[46] K. Levenberg, Q. Appl. Math. 2 (1944) 164.
[47] D. Marquardt, SIAM J. Appl. Math. 11 (1963) 431.
[48] I. Laaziz, A. Larbot, A. Julbe, C. Guizard, L. Cot, J. Solid State Chem. 98 (1992) 393.
[49] S. Doeuff, M. Henry, C. Sanchez, Mater. Res. Bull. 25 (1990) 1519.
[50] V. Torma, H. Peterlik, U. Bauer, W. Rupp, N. Hüsing, S. Bernstorff, M. Steinhart, G. Goerigk, U. Schubert, Chem. Mater. 17 (2005) 3146.
[51] T. Kamiyama, M. Mikami, K. Suzuki, J. Non-Cryst. Solids 150 (1992) 157.
[52] T.M. Stawski, S.A. Veldhuis, R. Besselink, H.L. Castricum, G. Portale, D.H.A. Blank, J.E. ten Elshof, J. Phys. Chem. C (2011), doi:10.1021/jp206572.
[53] J.A. Jutson, R.M. Richardson, S.L. Jones, C. Norman, 1990. In: B.J. Zelinski, C.J. Brinker, D.E. Clark, D.R. Ulrich, (Eds.), Better Ceramics through Chemistry IV, Mater. Res. Soc. Symp. Proc. 180, Mater. Res. Soc., Pittsburgh, p. 123.
[54] L.M. Toth, J.S. Lin, L.K. Felker, J. Phys. Chem. 95 (1991) 3106.
[55] A. Clearfield, Inorg. Chem. 3 (1964) 146.
[56] A. Clearfield, P.A. Vaughan, Acta Cryst. 9 (1956) 555.
[57] A. Clearfield, G.P.D. Serrette, A.H. Khazi-Syed, Catal. Today 20 (1994) 295.
[58] A. Singhal, L.M. Toth, J.S. Lin, K. Affholter, J. Am. Chem. Soc. 118 (1996) 11529.
[59] A. Singhal, L.M. Toth, G. Beaucage, J.S. Lin, J. Peterson, J. Colloid Interface. Sci. 194 (1997) 470.
[60] P. Riello, A. Minesso, A. Craievich, A. Benedetti, J. Phys. Chem. B 107 (2003) 3390.
[61] N. Rao, M.N. Holerca, M.L. Klein, V. Pophristic, J. Phys. Chem. A 111 (2007) 11395.
[62] A. Corina-Geiculescu, H.J. Rack, J. Non-Cryst. Solids 306 (2002) 30.
[63] N. Rao, M.L. Holerca, V. Pophristic, J. Chem. Theory Comput. 4 (2008) 145.
[64] D. Peter, T.S. Erstel, H. Bertagnolli, J. Sol–Gel Sci. Technol. 5 (1995) 5.